Solar Energy Materials & Solar Cells 132 (2015) 123–130

Contents lists available at ScienceDirect

Solar Energy Materials & Solar Cells

journal homepage: www.elsevier.com/locate/solmat

Tubular Si-infiltrated SiC_f/SiC composites for solar receiver application—Part 1: Fabrication by replica and electrophoretic deposition

A. Ortona [a], T. Fend [b], H.W. Yu [c], K. Raju [c], P. Fitriani [c], D.H. Yoon [c,1]

[a] ICIMSI, SUPSI, Galleria 2, CH-6928 Manno, Switzerland
[b] Institute of Solar Research, German Aerospace Center, Linder Höhe, 51147 Köln, Germany
[c] School of Materials Science and Engineering, Yeungnam University, Gyeongsan 712-749, Republic of Korea

ARTICLE INFO

Article history:
Received 30 May 2014
Received in revised form
4 August 2014
Accepted 24 August 2014

Keywords:
SiC_f/SiC composites
Replica method
Electrophoretic deposition
Reactive silicon-infiltration
Solar receiver
Concentrated solar energy

ABSTRACT

Tubular Si-infiltrated SiC_f/SiC composites composed of an inner cellular ceramic and an outer dense ceramic matrix composite (CMC) skin were fabricated by the electrophoretic deposition of matrix phases followed by Si-infiltration for solar receiver applications in concentrated solar energy. Using a combined replica method with the 3D printing of polymeric inks, 3 types of the inner cellular ceramics were produced to examine the permeability and heat transfer properties depending on their structure. To form a gastight dense skin layer, SiC fibers were layered on the cylindrical cellular ceramics by filament winding. The resulting preforms were infiltrated by electrophoretic deposition with SiC and carbon black particles and then by molten Si at 1550 °C. The fabrication process, resulting microstructure, and oxidation behavior of the composites at 1400 and 1600 °C in air are explained in Part 1. The thermophysical properties will be explained in Part 2. Overall, this hybrid method is a suitable processing technology for fabricating SiC_f/SiC-based solar receivers.

© 2014 Elsevier B.V. All rights reserved.

1. Introduction

SiC fiber-reinforced SiC matrix composites (SiC_f/SiC) have attracted considerable attention because of the increasing demand for toughened thermo-structural materials for high temperature applications. Compared to brittle monolithic ceramics, fiber-reinforced composites exhibit toughening behavior due to crack deflection, crack bridging, fiber pull-out and delamination mechanisms at the interface between the fibers and matrix [1]. Owing to its excellent mechanical, chemical and thermal properties along with low induced radioactivity under neutron radiation conditions, SiC_f/SiC can be used as structural materials for aerospace components, fusion and advanced fission reactors, and high temperature heat exchangers [2–5].

One of the most promising heat exchanger applications of SiC_f/SiC is the solar receiver for a concentrating solar power (CSP) plants, which generate electricity by direct concentration of solar radiation to produce steam or hot air for turbine operations [6,7]. The solar receivers are typically composed of internal porous channels to flow a liquid/gas medium and an outer gastight skin layer to protect the medium from leaking. Operation at higher temperature, high absorption in the visible and near infrared wavelength range, high thermal conductivity and porosity, and optimization of the geometrical structure of the solar receiver are essential to enhance the heat exchanging efficiency from the receiver to the medium [8]. Because the current metal-based receiver can only be operated at <600 °C [9], much higher heat transfer efficiency is expected if the SiC_f/SiC absorber with an inner SiC foam is implemented due to its possible operation at >1000 °C.

Two main barriers need to be solved before SiC_f/SiC can be implemented as a solar receiver. One is the fabrication technique for a tubular structure with porous open channels inside and a dense outside skin. The other one is the evaluation of thermophysical properties, such as the permeability and heat transfer properties, to verify the feasibility of SiC_f/SiC as a solar receiver. Regarding the formation of a porous body, direct foaming, gel casting and replica methods are used commonly for the production of reticulated random foams [10]. On the other hand, a rapid prototyping using a 3D printer with polymeric inks and slurry replica has been introduced recently, which can produce foam structures with the repeatable engineered pore size and shape [11]. Regarding matrix filling for a dense SiC_f/SiC skin fabrication, a range of techniques, such as chemical vapor infiltration, polymer impregnation and pyrolysis, slurry impregnation and liquid Si-infiltration, have been utilized so

E-mail address: dhyoon@ynu.ac.kr (D.H. Yoon).
[1] Tel.: +82 538102561; fax: +82 538104628.

http://dx.doi.org/10.1016/j.solmat.2014.08.029
0927-0248/© 2014 Elsevier B.V. All rights reserved.

far [1,12–16]. Although each process has its own advantages and disadvantages, Si-infiltration is known to be a fast and low-cost process. An inevitable presence of free Si in the composites produced by Si-infiltration can be minimized through the formation of reaction-bonded SiC from a reaction between the pre-infiltrated carbon powder and Si-melt. Moreover, electrophoretic deposition (EPD) combined with ultrasonic pulses was found to be quite effective in infiltrating matrix particles into the voids of woven SiC fiber preforms [17,18].

With these backgrounds, tubular Si-infiltrated SiC_f/SiC composites with an inner Si-infiltrated SiC foam and outer dense Si-infiltrated SiC_f/SiC skin were fabricated for use in high temperature heat exchangers, particularly for solar receiver applications in CSP. In this feasibility test, three different foam structures were prepared to compare the thermal exchanging efficiency depending on the foam structures using a conventional replica method and recently available prototyping using a 3D printer. This report is composed of two parts. Part 1 (the present paper) focuses mainly on the fabrication techniques for tubular Si-infiltrated SiC_f/SiC composites along with the oxidation behavior at $\geq 1400\ ^\circ C$ in air. Part 2 explains the thermophysical properties of the tubular composites for solar receiver applications.

2. Materials and methods

2.1. Foam preparation and filament winding

Three types of Si-infiltrated SiC macro-porous ceramics were fabricated to compare the thermal exchanging efficiency upon their morphological differences, as shown in Fig. 1. One was a reticulated random foam produced by a replica method with a 5–6 mm pore size, which is equivalent to 8 ppi (pores/inch). The others were periodic cellular ceramics produced by 3D printing (Eden 260V, Object Ltd., Israel), where each pore had approximately $2 \times 2 \times 3\ mm^3$ dimensions. After designing the geometry shown in Fig. 1(b) and (c) using a software (HyperMesh, Altair HyperWorks, USA), the templates were 3D-printed with photosensitive resins (Fullcure 705 and 850 VeroGray, Object Ltd.), which were composed of acrylics, urethanes and epoxies. Both resins were compounded with a photo-initiator that triggered the polymerization under UV light. The 3D printing was performed with the minimum resolutions of 16 and 42 μm for vertical and planar directions, respectively. After removal the surface resin with a water jet, the templates were replicated using SiC slurry. As shown in the top-view images in Fig. 1(b) and (c), two types of periodic lattices differed by the spiral angles of the third layer, i.e. one had a straight channels while the other had a swirled channel structure with a 45° helical angle. The samples were named as R-, N- and S-sample for convenience depending on the structure of porous ceramics for random, straight and swirled, respectively. Replica was performed by SiC slurry impregnation, pyrolysis at 1000 °C for 1 h and Si-infiltration at 1500 °C. More detailed fabrication steps for the periodic cellular foam can be found elsewhere [11]. All samples had a cylindrical shape with a diameter of 20 mm and a height of 40 mm. The surface area of the R-sample was $69\ cm^2$/sample and that of the N- and S-sample was $85\ cm^2$/sample because of their smaller cell size.

SiC fibers (Tyranno™ SAX-S1I16PX, Ube Industries Ltd., Japan) were wound around the cylindrical Si-infiltrated SiC foam to form a skin layer. The yarn for winding was composed of 1600 fibers with a diameter of 7.5 μm. Winding was carried out on a lathe after fixing the cylindrical foam at a rotating spindle chuck, while the yarn carriage was moved automatically from side to side

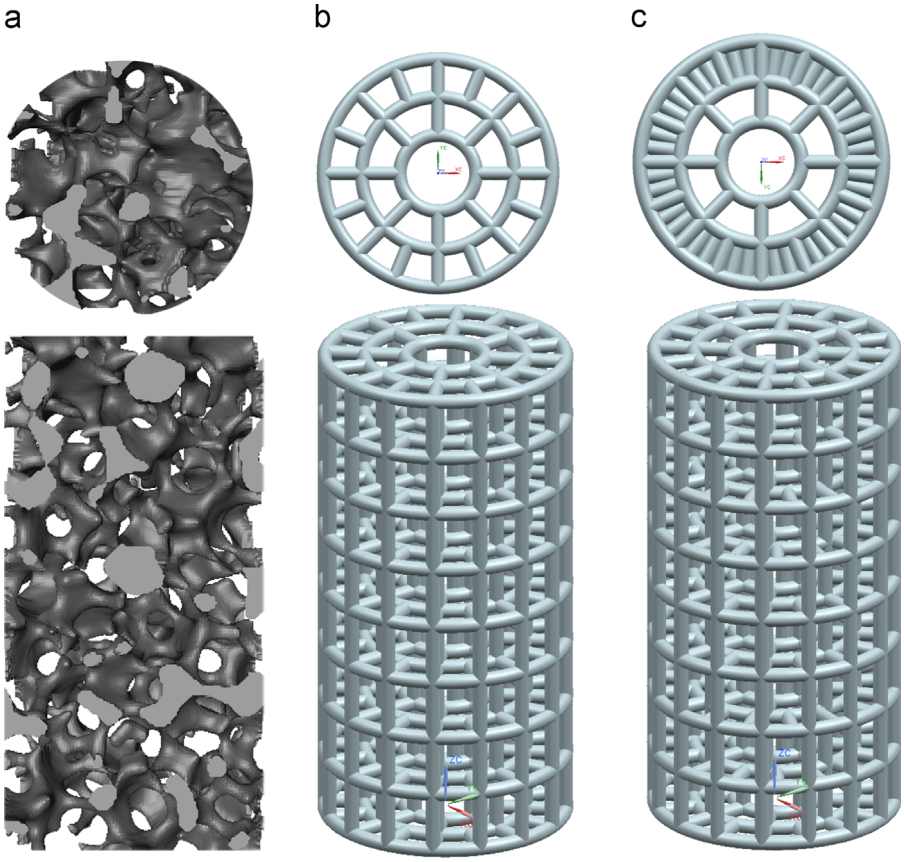

Fig. 1. Schematic diagram of the top-view (upper) and side-view (lower) of the (a) random (R), (b) straight (N), and (c) swirled (S) samples. Each sample had a diameter of 20 mm and height of 40 mm.

for precise winding. Six layers of SiC yarn was wound on the sample with a helical angle of 2° and a pitch of 2.0 mm approximately. A liquid phenolic resin was applied between the layers for adhesion. Samples were pyrolyzed at 960 °C for 2 h in an Ar atmosphere.

2.2. Electrophoretic deposition and Si-infiltration

Forty grams of β-SiC (mean particle size (D_m)=52 nm, purity >97.5%, 4620KE, NanoAmor Inc., USA) and 20 g of carbon black (D_m=50 nm, purity >98.5%, HiBlack 50L, Shin Woo Materials, Korea) powders were dispersed in ethanol, which contained 3 g of a polyester/polyamine co-polymeric cationic dispersant (Hypermer KD1, ICI, UK) and 3 g of a polyvinyl butyral binder (PVB, Butvar B-98, M_w=55,000 g/mol, Solutia, USA). The slurry was ball-milled for 24 h using 6 mm SiC balls to ensure particle dispersion.

Electrophoretic deposition (EPD) was carried out on the sample to infiltrate the matrix phase composed of SiC and carbon black particles into the voids of the fiber skin. The foam was filled with a molten wax before EPD to prevent unwanted deposition of the matrix phase onto the struts. DC 10 V was applied for 1 h under 10 W ultrasonic pulses at 60 Hz for the first 50 min to minimize preferential deposition at the surface of the skin. After removing the wax from the cylindrical sample at 80 °C in air, binder burnout was performed at 350 °C for 2 h in a N_2 atmosphere.

Si-infiltration was performed at 1550 °C for 10 min under a pressure of 10^{-2} mbar after placing 6.5 g of Si lumps on top of the cylindrical sample based on the preliminary test results. Coarse Si lumps (D_m=2.5 mm, >99.99% pure, Worldex, Korea) were used, while the cylindrical sample was placed on boron nitride-painted graphite wicks to drain the excess molten Si.

2.3. Oxidation test

The oxidation test was performed on the surface-polished R-, N- and S-samples at 1400 and 1600 °C, respectively, in flowing dry air (500 ml/min). Samples were heated up at a heating rate of 5 °C/min, kept at the target temperature for 24 h and then furnace-cooled. Weight and microstructural changes as well as surface phase evolution upon oxidation were analyzed.

2.4. Characterization

The samples were characterized using a variety of techniques. The zeta potentials of SiC and carbon black particles in ethyl alcohol containing a dispersant were measured using an electroacoustic-type zeta potential analyzer (Zeta Probe, Colloidal Dynamics, USA) after adjusting the operational pH of the suspension with NH_4OH and HCl.

The morphology of the starting materials and consolidated bodies were observed by scanning electron microscopy (SEM: S-4800, Hitachi at 15 kV and 10 μA). Energy dispersive X-ray spectrometry (EDS: Horiba EX-250) combined with SEM was used to examine the composition of each phase after Si-infiltration. The density was measured using the Archimedes method, and the phase generated during the Si-infiltration and oxidation test was determined from a Rietveld simulation using X-ray diffraction (XRD: X'Pert-PRO MPD, Pananalytical using Cu $K\alpha$ line, 40 kV and 30 mA) patterns. The weight change upon the oxidation test was measured using a scale accurate to 0.1 mg. After cutting the skin layer into $4 \times 2 \times 40$ mm^3 pieces from a tube, a 3-point bending test (UTM AG-50E, Shimadzu, Japan) was performed for 5 samples at a crosshead speed of 0.5 mm/min and a span of 30 mm.

3. Results and discussion

The Si-infiltrated SiC cellular ceramics (Fig. 1) are expected to be well-suited for solar receiver applications in CSP because of the high heat conductivity of their constituent materials, large surface area for enhanced heat exchanging properties and low pressure drop due to their open structures. In addition, operation at higher temperature along with a longer lifetime than the metal-based foams is also anticipated because of the high corrosion/oxidation resistance of the ceramic-based foams. The issues associated with the present fabrication of ceramic lattices could be solved using a 3D printing followed by replica. Fig. 2(a) shows an image of the N-sample fabricated using the replica method combined with 3D printing, which had a high surface area of 85 cm^2/sample and 25 cells on its cross-section to confer a high heat exchanging efficiency. For the flowing of the liquid/gas media through the porous body without leaking, a gastight skin layer was formed around the porous body by SiC filament winding and subsequent infiltration of carbon black and SiC particles followed

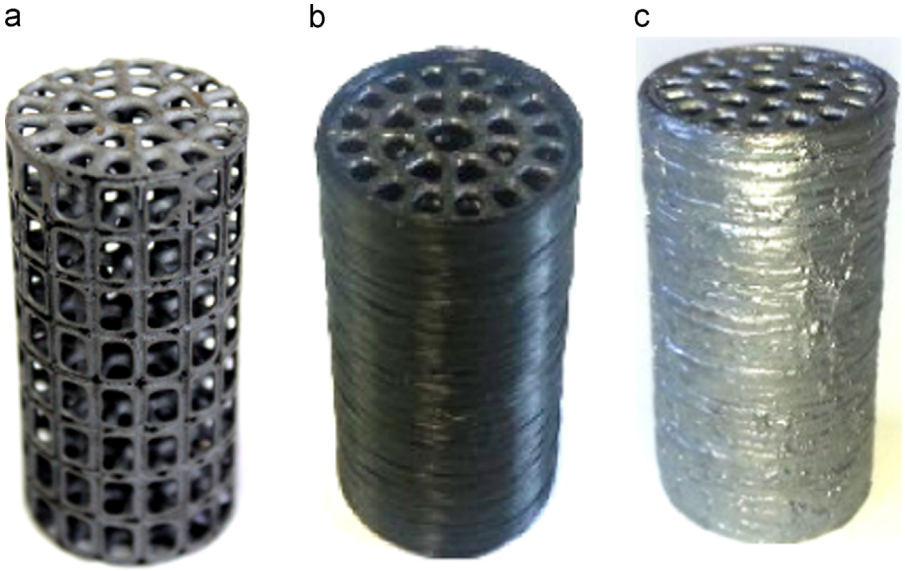

Fig. 2. Digital camera images of the N-sample: (a) periodic foam lattice by replica method combined with 3D printing, (b) after filament winding using a Tyranno fiber, and (c) final sample treated with EPD followed by Si-infiltration.

by Si-infiltration. Fig. 2(b) and (c) present images of the filament-wound and final Si-infiltrated N-sample, respectively.

Although a dense skin layer might be formed solely by Si-infiltration, the electrophoretic infiltration of SiC and carbon black particles into the voids of the SiC fiber-wound was performed before Si-infiltration. Because SiC has higher thermal conductivity and stability than Si, the relative content of SiC in the composite can be increased by the infiltration of SiC, even though the presence of free Si is inevitable with Si-infiltration process. Moreover, the formation of reaction-bonded SiC can be expected by a reaction between the infiltrated carbon powder and Si-melt because of the negative Gibbs formation free energy: −53 kJ/mol for SiC formation from Si and C at 1550 °C [19]. Fig. 3(a) shows a schematic design of the EPD apparatus, which is comprised of a positive electrode connected to a cylindrical stainless steel container, a negative electrode connected to the R-, N-, and S-sample located at the center of the container after filling the pores with a molten wax, and a ceramic slurry dispersed in ethyl alcohol. Ultrasonic pulses, 10 W at 60 Hz, were applied for the first 50 min during 1 h of EPD to minimize the preferential deposition of ceramic particles at the surface of the SiC fiber layer without infiltrating into the deep voids of the fiber layer. The effects of ultrasonication on the degree of infiltration into the fine voids of SiC fabrics are reported elsewhere [17]. Because EPD uses the migration of charged particles dispersed in a liquid medium onto the conducting substrate of an opposite charge under a DC electric field, the zeta potential of SiC and carbon black particles is very important for determining the direction of deposition and the particle mobility. Fig. 3(b) shows the zeta potential vs. operational pH behavior of each 10 wt% SiC and carbon black slurry after adding a commercial dispersant. Both particles showed a typical zeta potential behavior with the change in operational pH, i.e. increase in the zeta potential by decreasing the operational pH due to the increase in H^+ ions. The rheological and zeta potential behavior upon the addition of PVB binder and dispersant can be found in a previous report [18]. The operational pH of the slurry was set to 4 for EPD by considering the zeta potential results shown in Fig. 3(b). Because both particles migrate to the negative electrode due to the positive zeta potential under this condition, each of R-, N- and S-samples were connected to the negative electrode, as shown in Fig. 3(a). Although the zeta potential of carbon black at an operational pH 4 was as low as 15 mV, the electrophoretic mobility was sufficient to deposit carbon black onto the negative electrode based on the preliminary test, which might be due to the fine particle size (D_m=50 nm). Fig. 4(b) shows a SEM image of the layer deposited onto the SiC fiber winding by EPD. The ceramic particles deposited well, even though there were drying cracks, as shown in Fig. 4(a). According to the measurement, a 1.03 ± 0.04 g weight increase was observed by EPD for the samples weighing 8.22 ± 0.56 g, which corresponds to a 12.59% weight gain.

Fig. 5 shows SEM images of the polished surface for R-, N- and S-samples after Si-infiltration, showing an outside skin layer, inside foam and the interface between them. The thickness of the skin layer was approximately 1 mm, which can be distinguished by traces of SiC fibers with a dark gray color. The phase with a light gray color in the skin layer corresponds to free-Si, based on further analysis using EDS. Both the skin and foam of the three types of samples showed a dense morphology without the presence of small

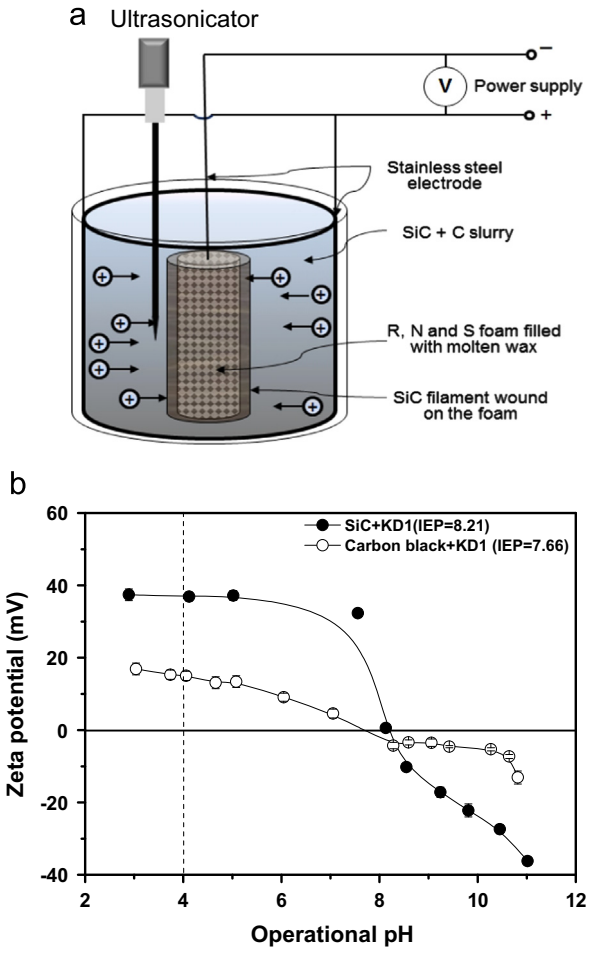

Fig. 3. (a) Schematic diagram of electrophoretic deposition combined with ultrasonication used for the matrix particle infiltration and (b) zeta potential vs. operational pH behavior of the 10 wt% β-SiC and carbon black slurry with a commercial dispersant (KD1) in ethyl alcohol. Both modified from [3].

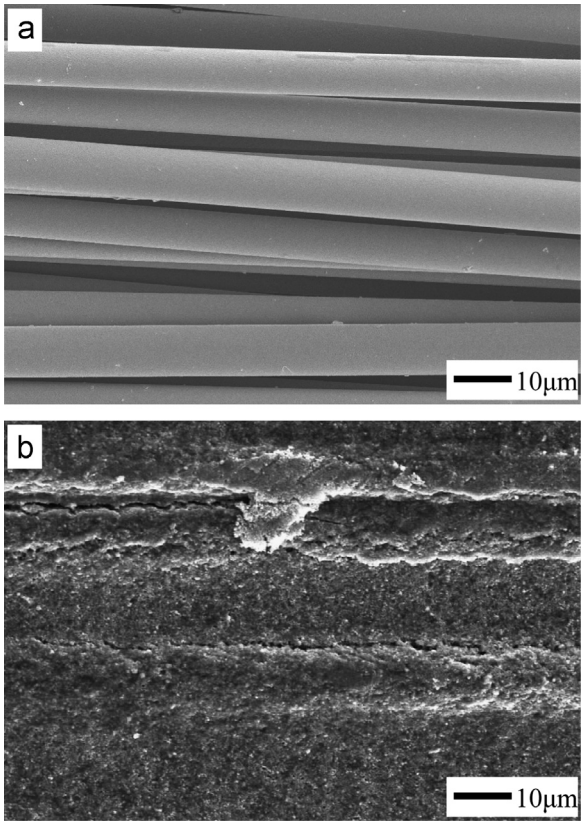

Fig. 4. SEM images of the SiC filaments-wound skin layer (a) before and (b) after SiC and carbon black infiltration using electrophoretic deposition combined with ultrasonic pulse application.

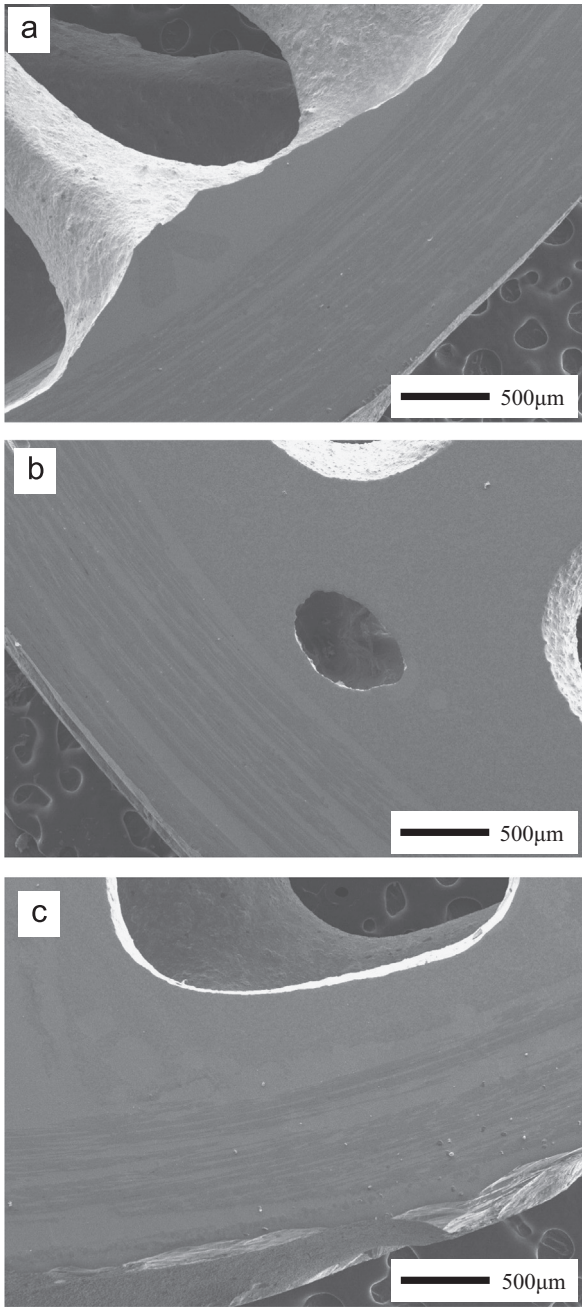

Fig. 5. SEM images of the polished surface for (a) R-, (b) N- and (c) S-sample, showing a tight joint between the skin and foam.

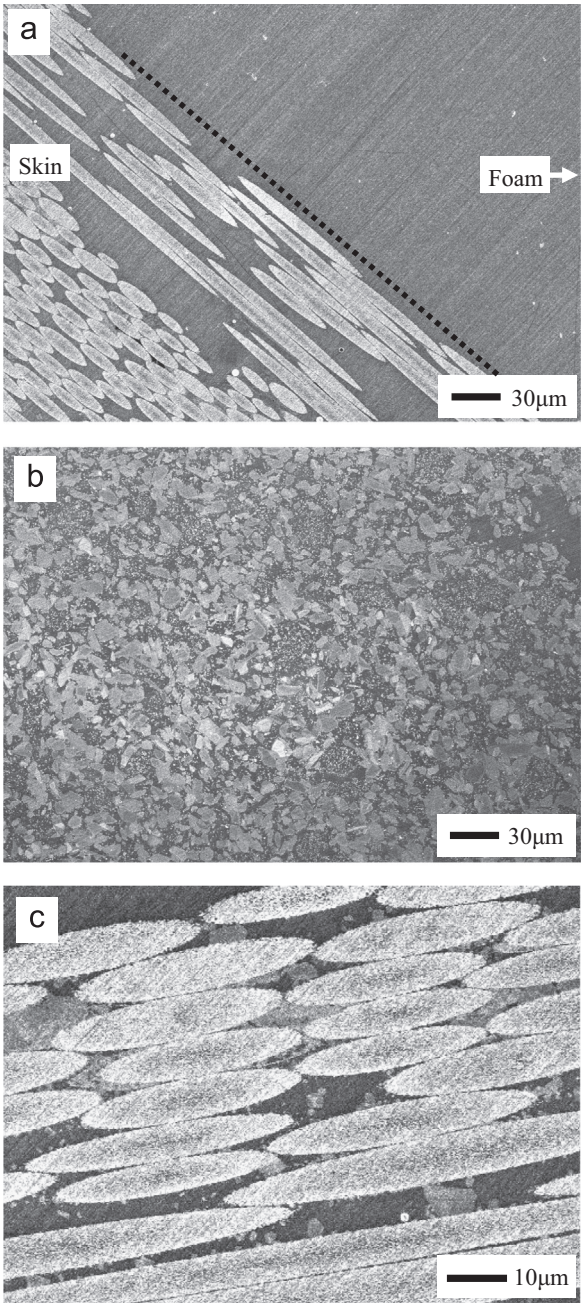

Fig. 6. SEM images of the N-sample for (a) interface, (b) foam and (c) skin layer showing the presence of SiC and Si between the SiC fibers.

pores along with the large cells formed by the struts. Tight joining between the foam and skin layer was observed for all samples, where heat transfer occurs from the skin layer, which receives solar radiation, to the inside foam. A dense interface would be desirable to maximize the heat exchanging efficiency. The other important thing is the smooth foam surface, which can minimize the pressure drop and maximize the heat transfer efficiency to the liquid/gas media. According to the foam surface morphology shown in Fig. 5, all samples revealed relatively smooth strut surface. The density of the foams was 2.65 ± 0.03 g/cm^3, whereas that for the skin was 2.74 ± 0.02 g/cm^3, regardless the type of the sample. The higher density of the skin was attributed to the larger SiC content due to the SiC fibers than the foam because SiC has a higher theoretical density ($=3.22$ g/cm^3) than Si ($=2.33$ g/cm^3).

Fig. 6 shows the polished surface image of the N-sample at a higher magnification than that of Fig. 5. The presence of SiC fibers with an elliptical shape and a well-joined interface can be seen clearly in Fig. 6(a). The foam shown in Fig. 6(b) showed a large number of SiC particles embedded in the Si matrix. A more elaborate image for the skin layer shown in Fig. 6(c) revealed the presence of a SiC matrix phase between the fibers distinguished by a light gray color, which was formed by a reaction between carbon black and the Si-melt at high temperatures or SiC particle infiltration by EPD.

Fig. 7 shows the XRD pattern of the Si-infiltrated SiC_f/SiC skin layer for the R-sample, which is composed of free Si, β-SiC and SiO_2. According to Rietveld analysis for the whole R-, N- and S-samples, the amounts of Si, β-SiC and SiO_2 were 32.7–35.3, 63.2–66.2 and 0.8–2.7 wt%, respectively. Although the peak height for Si

was larger than that of SiC, more SiC existed in the composite, based on the Rietveld analysis. The presence of SiO_2 was attributed to oxidation of the Si and SiC surface. A larger portion of SiC in the composite is desirable because the thermal conductivity of SiC (=3.2 W/cm K) is larger than that of Si (=1.5 W/cm K at 300 K) [20].

Based on the 3-point bending test, the mean flexural strength for the skin was 160.3 ± 27.6 MPa, which is believed to confer sufficient strength for solar absorber applications. To enhance the strength of the skin layer, however, a thicker skin layer and the formation of weak interfacial layer on the SiC fibers, such as a pyrolytic carbon coating to maximize the toughening mechanism, might be considered.

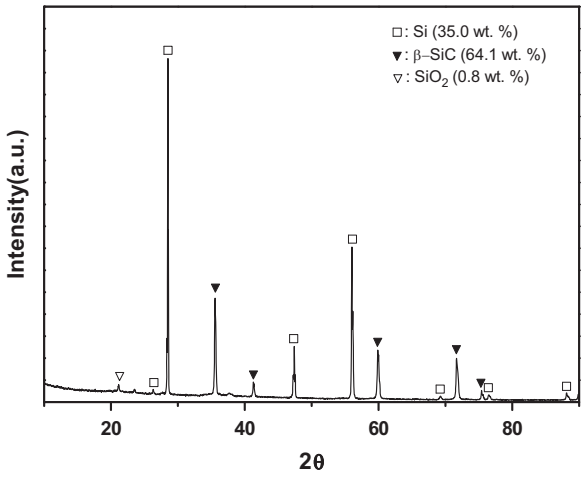

Fig. 7. XRD pattern of the Si-infiltrated SiC_f/SiC skin layer of the R-sample. The values in parenthesis indicate the wt% of each phase based on a Rietveld simulation.

The oxidation test at 1400 and 1600 °C for 24 h in air revealed a weight gain of 0.60 ± 0.03% and 0.93 ± 0.04%, respectively. Fig. 8 shows SEM images of the N-sample after oxidation at 1400 and 1600 °C for the skin and foam along with the composition of the surface, based on EDS area analysis for the region indicated with the rectangle. Compared to the SEM images shown in Fig. 6 for the same sample prior to oxidation, which revealed the clear distribution of SiC fibers, Si and SiC in the matrix, the polished samples after oxidation showed a surface layer, as shown in Fig. 8. This layer was composed mainly of oxygen and Si, which was believed to be SiO_2, based on EDS analysis. SiC is known to be oxidized forming a condensed SiO_2(s) or volatile SiO(g), depending on the oxygen partial pressure, impurity level and temperature [21]. The formation of SiO_2 is termed 'passive oxidation,' protecting further oxidation of SiC based on the following reaction:

$$SiC(s)+3/2O_2(g)=SiO_2(s)+CO(g)$$

On the other hand, the formation of SiO is termed 'active oxidation,' leading a rapid weight loss based on the following reaction:

$$SiC(s)+O_2(g)=SiO(g)+CO(g)$$

SiC forms a passive SiO_2 layer at relatively low temperatures, which prevents further oxidation of SiC by blocking oxygen diffusion through this layer. In contrast to Si, which shows passive oxidation up to its melting point, SiC showed an active oxidation at high temperatures by forming gaseous SiO rather than solid SiO_2, accompanying a drastic weight decrease [21]. Although this passive-to-active transition was reported to occur

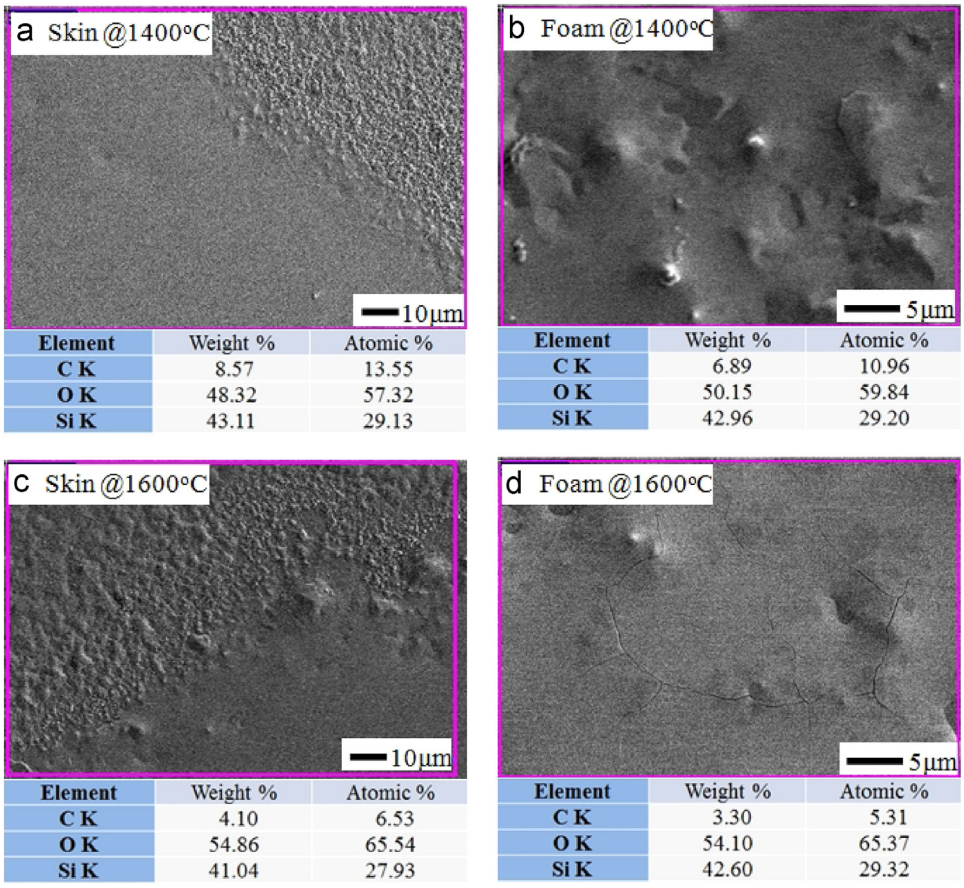

Element	Weight %	Atomic %
C K	8.57	13.55
O K	48.32	57.32
Si K	43.11	29.13

Element	Weight %	Atomic %
C K	6.89	10.96
O K	50.15	59.84
Si K	42.96	29.20

Element	Weight %	Atomic %
C K	4.10	6.53
O K	54.86	65.54
Si K	41.04	27.93

Element	Weight %	Atomic %
C K	3.30	5.31
O K	54.10	65.37
Si K	42.60	29.32

Fig. 8. SEM images of the N-sample after the oxidation test at 1400 and 1600 °C for 24 h. The EDS area analysis results for each condition are shown in the lower part of the image.

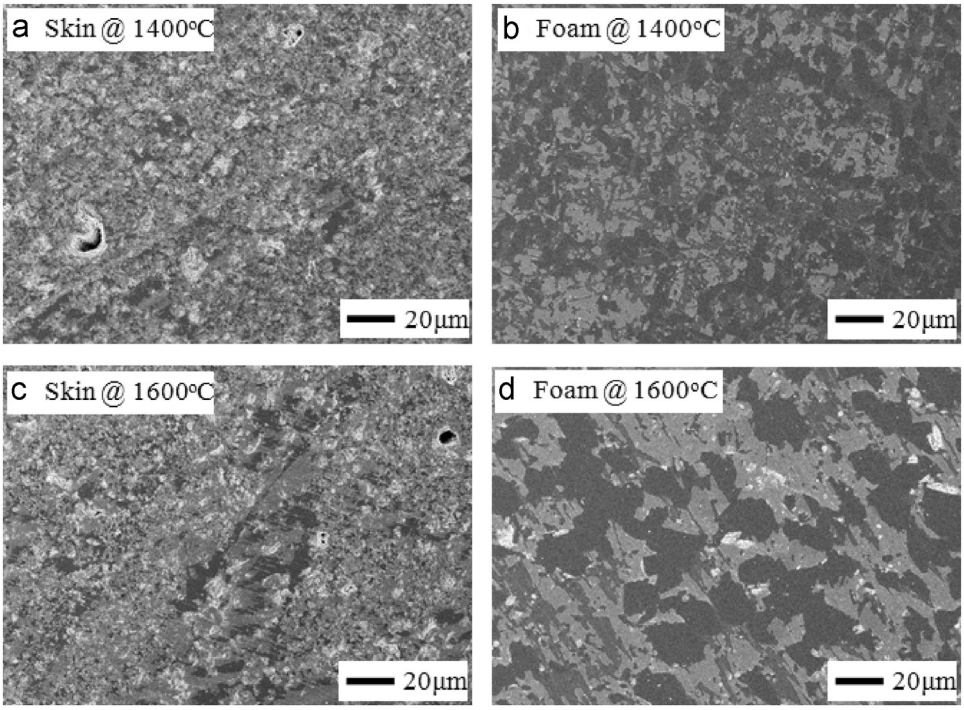

Fig. 9. SEM images of the polished N-sample showing the morphology of the skin and foam after oxidation at 1400 and 1600 °C for 24 h.

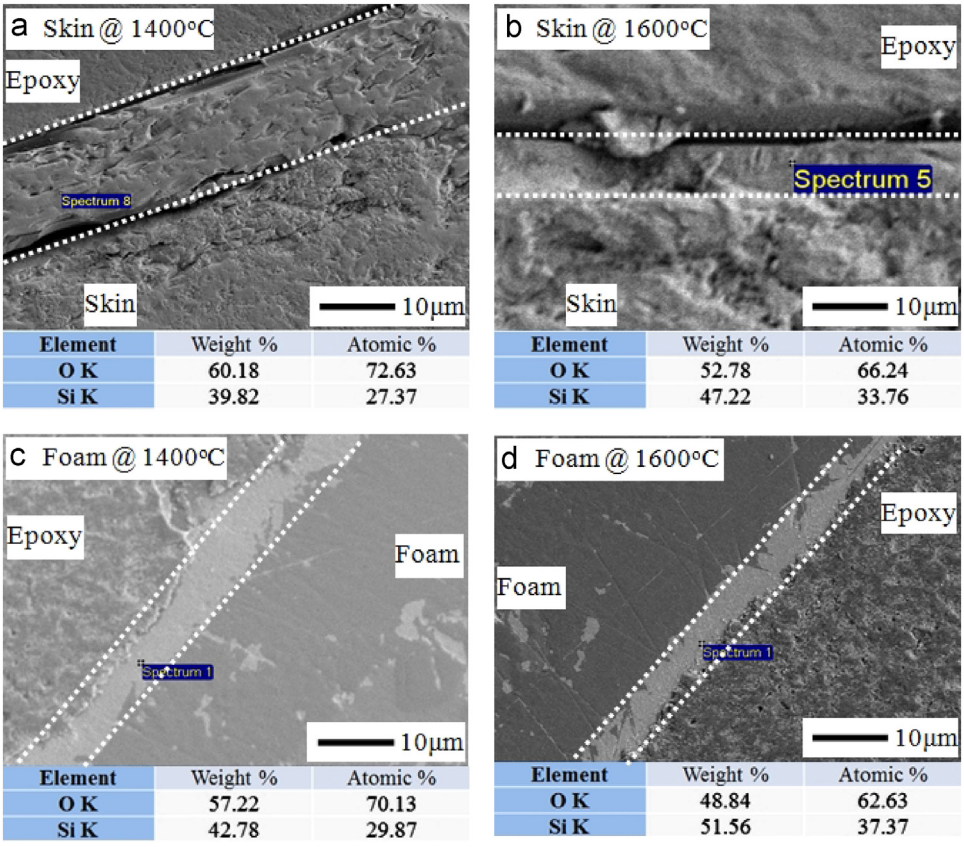

Element	Weight %	Atomic %
O K	60.18	72.63
Si K	39.82	27.37

Element	Weight %	Atomic %
O K	52.78	66.24
Si K	47.22	33.76

Element	Weight %	Atomic %
O K	57.22	70.13
Si K	42.78	29.87

Element	Weight %	Atomic %
O K	48.84	62.63
Si K	51.56	37.37

Fig. 10. SEM images for the skin and foam of N-sample after the oxidation test at 1400 and 1600 °C along with the EDS point analysis results shown in the lower part of each image.

at high temperatures, the EDS results in shown Fig. 8 revealed a stoichiometric SiO_2 composition approximately, indicating that there was no passive-to-active transition in our experimental conditions.

Fig. 9 shows SEM images of the polished N-sample for the skin and foam after oxidation. Although the skin layer shows the presence of small closed pores, it is believed that the gas tightness of the skin layer is maintained regardless the exposure

temperatures, based on the microstructure. However, the presence of SiC fiber at the skin layer cannot be found after oxidation because of the reaction between the SiC fiber and matrix phase. This reaction could be avoided by the coating of interphase layer on the SiC fiber, such as pyrolytic carbon or boron nitride, based on the previous results [15,17]. On the other hand, the foam shows dense morphology without the presence of pore and reveals the grain growth of both Si and SiC by increasing the temperature from 1400 to 1600 °C. The light and dark phases in Fig. 9 (d) correspond to Si and SiC, respectively. It is notable that both of the skin and foam maintain dense microstructure after exposure at 1600 °C, which is higher than the melting point of Si (1420 °C). This could happen by the formation of dense SiO_2 passive layer on the sample surface during the high temperature exposure.

Fig. 10 shows the SiO_2 layer on the surface of skin and foam after oxidation along with the EDS analysis results for the point marked with 'spectrum.' Molding using an epoxy was performed before polishing to preserve the SiO_2 layer. All samples show a 6–14 μm thick dense SiO_2 passivation layer by oxidation at 1400 and 1600 °C for 24 h in air, according to the stoichiometry of the EDS point analysis results.

4. Conclusions

To test the feasibility of Si-infiltrated SiC_f/SiC composite tubes for solar absorber applications, three types porous cellular ceramics with different morphologies were prepared: one reticulated random foam (R-type) and two lattice structures (N- and S-type) with different spiral angles produced by 3D printing combined with a replica method. A gastight dense Si-infiltrated SiC_f/SiC composite skin layer was formed by the EPD of carbon black and SiC particles followed by Si-infiltration at 1550 °C for 10 min for the SiC fiber-wound layer. All tubular samples showed dense CMC skins, which were tightly joined to the inner porous ceramic body, ensuring high heat exchanging efficiency and mechanical properties. Moreover, the use of carbon black and ultrasonic pulses for EPD resulted in the formation of a reaction-bonded β-SiC phase between the SiC fibers, increasing the relative amount of SiC with higher thermal conductivity than Si. The skin layer was composed of 32.7–35.3, 63.2–66.2 and 0.8 – 2.7 wt% of free Si, β-SiC and SiO_2, respectively, along with a flexural strength of approximately 160 MPa. The oxidation at 1400 and 1600 °C for 24 h in air revealed a 6–14 μm thick dense SiO_2 passivation layer on the composite surface, which prevented further oxidation. The overall microstructural, mechanical and oxidation properties indicated that this hybrid method would be a suitable fabrication technique for producing SiC_f/SiC-based solar absorbers, suggesting possible practical applications by increasing the sample dimension. In the second part of this report (part 2), the thermophysical properties of these samples will be explained.

Acknowledgements

This study was supported by The KORANET (www.koranet.eu) Joint Call on Green Technologies (Grant no. NRF-2012K1A3-A7A03051754), by The Basic Science Research Program through the National Research Foundation of Korea (NRF) funded by The Ministry of Education, Science and Technology (Grant no. 2012R1A1A2000858), and by The Swiss National Science Foundation (Grant no. IZ11Z0-145220).

References

[1] S. Dong, Y. Katoh, A. Kohyama, Preparation of SiC/SiC composites by hot pressing, using Tyranno-SA fiber as reinforcement, J. Am. Ceram. Soc. 86 (2003) 26–32.
[2] B. Riccardi, L. Giancarli, A. Hasegawa, Y. Katoh, A. Kohyama, R.H. Jones, L. L. Snead, Issues and advances in SiC_f/SiC composites development for fusion reactors, J. Nucl. Mater. 329–333 (2004) 56–65.
[3] B. Riccardi, P. Fenici, A.F. Rebelo, L. Giancarli, G.L. Marois, E. Philippe, Status of the European R&D activities on SiC_f/SiC composites for fusion reactors, Fusion Eng. Des. 51–52 (2000) 11–22.
[4] S.J. Dapkunas, Ceramic heat exchangers, Am. Ceram. Soc. Bull. 67 (1988) 388–391.
[5] A. Sommers, Q. Wang, X. Han, C. T'Joen, Y. Park, A. Jacobi, Ceramics and ceramic matrix composites for heat exchangers in advanced thermal system—a review, Appl. Therm. Eng. 30 (2010) 1277–1291.
[6] M. Thirugnanasambandam, S. Iniyan, R. Goic, A review of solar thermal technologies, Renewable Sustainable Energy Rev. 14 (2010) 312–322.
[7] H. Müller-Steinhagen, F. Trieb, Concentrating solar power, Ingenia 18 (2004) 43–50.
[8] T. Fend, B. Hoffschmidt, R. Pitz-Paal, O. Reutter, P. Rietbrock, Porous materials as open volumetric solar receivers: experimental determination of thermophysical and heat transfer properties, Energy 29 (2004) 823–833.
[9] N. Michailidis, F. Stergioudi, H. Omar, D. Missirlis, Z. Vlahostergios, S. Tsipas, C. Albanakis, B. Granier, Flow, thermal and structural application of Ni-foam as volumetric solar receiver, Sol. Energy Mater. Sol. Cells 109 (2013) 185–191.
[10] J.H. Eom, Y.W. Kim, S. Raju, Processing and properties of macroporous silicon carbide ceramics: a review, J. Asian Ceram. Soc. 1 (2013) 220–242.
[11] A. Ortona, C. D'Angelo, S. Gianella, D. Gaia, Cellular ceramics produced by rapid prototyping and replication, Mater. Lett. 80 (2012) 95–98.
[12] R. Yamada, T. Taguchi, N. Igawa, Mechanical and thermal properties of 2D and 3D SiC/SiC composites, J. Nucl. Mater. 283–287 (2000) 574–578.
[13] C.A. Nannetti, A. Ortona, D.A. de Pinto, B. Riccardi, Manufacturing SiC-fiber—reinforced SiC matrix composites by improved CVI/slurry infiltration/polymer impregnation and pyrolysis, J. Am. Ceram. Soc. 87 (2004) 1205–1209.
[14] J.C. Margiotta, D. Zhang, D.C. Nagle, C.E. Feeser, Formation of dense silicon carbide by liquid silicon infiltration of carbon with engineered structure, J. Mater. Res. 23 (2008) 1237–1248.
[15] P. Yonathan, J.H. Lee, D.H. Yoon, W.J. Kim, J.Y. Park, Improvement of SiC_f/SiC density by slurry infiltration and tape stacking, Mater. Res. Bull. 44 (2009) 2116–2122.
[16] D.W. Shin, S.S. Park, Y.H. Choa, K. Niihara, Silicon/silicon carbide composites fabricated by infiltration of a silicon melt into charcoal, J. Am. Ceram. Soc. 82 (1999) 3251–3253.
[17] G.Y. Gil, D.H. Yoon, Densification of SiC_f/SiC composites by electrophoretic infiltration combined with ultrasonication, J. Ceram. Proc. Res. 12 (2011) 371–375.
[18] A. Ortona, T. Fend, H.W. Yu, K. Raju, D.H. Yoon, Fabrication of cylindrical SiC_f/Si/SiC-based composites by electrophoretic deposition and liquid silicon infiltration, J. Eur. Ceram. Soc. 34 (2014) 1131–1138.
[19] I. Barin, Thermochemical Data of Pure Substances—Part II, VCH, NY (1989) 1342.
[20] H. Abderrazak, E. Selmane, B.H. Hmida, in: R. Gerhardt (Ed.), Silicon Carbide: Synthesis and Properties in Properties and Applications of Silicon Carbide, InTech, Croatia, 2011, pp. 362–363.
[21] N.S. Jacobson, D.L. Myers, Active oxidation of SiC, Oxid. Met. 75 (2011) 1–25.